
A DEEP CONVOLUTIONAL NEURAL NETWORK FOR SALT-AND-PEPPER NOISE REMOVAL USING SELECTIVE CONVOLUTIONAL BLOCKS

A PREPRINT

 **Ahmad Ali Rafiee**

Department of Electronics and
Telecommunications Engineering
Shiraz University
Shiraz, Iran
aa.rafiie@shirazu.ac.ir

 **Mahmoud Farhang**

Department of Electronics and
Telecommunications Engineering
Shiraz University
Shiraz, Iran
mfarhang@shirazu.ac.ir

ABSTRACT

In recent years, there has been an unprecedented upsurge in applying deep learning approaches, specifically convolutional neural networks (CNNs), to solve image denoising problems, owing to their superior performance. However, CNNs mostly rely on Gaussian noise, and there is a conspicuous lack of exploiting CNNs for salt-and-pepper (SAP) noise reduction. In this paper, we proposed a deep CNN model, namely SeConvNet, to suppress SAP noise in gray-scale and color images. To meet this objective, we introduce a new selective convolutional (SeConv) block. SeConvNet is compared to state-of-the-art SAP denoising methods using extensive experiments on various common datasets. The results illustrate that the proposed SeConvNet model effectively restores images corrupted by SAP noise and surpasses all its counterparts at both quantitative criteria and visual effects, especially at high and very high noise densities.

Keywords Image denoising · Salt-and-pepper noise · Selective convolutional block · Convolutional neural network · Deep learning · Edge preservation · Very high noise density

1 Introduction

Images are polluted by miscellaneous types of noises during acquisition, compression, and transmission. The resulting image information loss and poor quality of images give rise to considerable difficulties for many other image processing and computer vision tasks [1–3]. Therefore, image denoising is considered a classical yet still vital low-level vision issue, and is a basic necessity in many computer vision applications. The image denoising process aims to remove noise from noisy images along with retaining the edges, textures, and details of images, which leads to obtaining denoised images with superior quality [4]. Impulse noise is one of the prevalent types of noise in images that changes the value of some randomly selected pixels in images. Impulse noise can be classified into two categories, i.e., salt-and-pepper (SAP) noise and random-valued noise. In the presence of SAP noise, noisy pixels take the maximum value (i.e., 255 in 8-bit images) with a probability of D_s or the minimum value (0) with a probability of D_p , which are respectively

referred to as the salt noise (white dots) and the pepper noise (black dots) [5]. The probability density function (PDF) of SAP noise in the 8-bit gray-scale images is given by [5]:

$$p(z) = \begin{cases} D_s & \text{for } z = 255 \\ D_p & \text{for } z = 0 \\ 1 - D & \text{for } z = \nu \end{cases} \quad (1)$$

where z represents intensity of the image and ν is any integer value such that $0 < \nu < 255$. D_s and D_p denote the probability of pixel corruption by salt noise and pepper noise, and $D = D_s + D_p$ is the noise density. Usually, D_s and D_p are considered equal.

Many attempts have been hitherto suggested for SAP denoising ([6–14]). Attributed to the fact that corrupted pixels by SAP noise are the maximum or minimum values of noisy images, median-based filter approaches have received considerable attention as the starting point of the efforts to remove SAP noise. The classic median filter (MF) [1], adaptive median filter (AMF) [15], decision-based algorithm (DBA) [16], modified decision based unsymmetric trimmed median filter (MDBUTMF) [7] can be mentioned as the most famous traditional median-based filter methods. These primitive methods generally encounter formidable obstacles to eliminating SAP noise, particularly at high noise densities in which almost all the pixels in the local window are noisy [2, 6, 8]. They also suffer from blurring the details and edges of the images and producing streaking effects [17, 18].

Several algorithms using novel interpolation techniques have been recently developed with the aim of alleviating these restrictions by image information preservation and visual quality improvement, particularly in the presence of high-density noises. Some approaches use mean-based filters on non-noisy (clean) pixels in a local window to restore noisy pixels. Adaptive weighted mean filter (AWMF) [8] and its modified versions—e.g., adaptive switching weight mean filter (ASWMF) [19] and improved adaptive weighted mean filter (IAWMF) [20]—restore noisy pixels by using various weighting methods to calculate the weighted average of non-noisy pixels in an adaptive window. Riesz mean is another average-based technique that has met with success in SAP noise removal. This technique is employed in the pixel similarity-based adaptive Riesz mean filter (ARmF) [21] and the different adaptive modified Riesz mean filter (DAMRmF) [22]. There are also some approaches that adopt mean-based or median-based filters or a combination of both in multiple stages to denoise images. The different applied median filter (DAMF) uses two consecutive median filters. In contrast to DAMF, adaptive Cesáro mean filter (ACmF) [23] employs the Cesáro mean instead of the median in a recursive algorithm which improves performance but decreases the execution time. In [24], a four-stage median-average (FoMA) algorithm is introduced, employing four-step median and mean filters.

Kriging interpolation is another interpolation technique utilized for SAP noise reduction. The adaptive decision based Kriging interpolation filter (ADKIF) [9] can achieve good results by employing Kriging interpolation. Besides the aforementioned methods, a multistage selective convolution filter (MSCF) was recently proposed in [25], which could significantly reduce the computation time along with a considerable noise suppression performance. Finally, an impulse denoising method based on noise accumulation and harmonic analysis techniques (NAHAT) [26] could achieve the best SAP denoising performance among non-deep learning-based algorithms by employing noise accumulation and solving a system of equations corresponding to a harmonic function.

Recent years have seen greater emphasis than heretofore on the application of machine learning methodologies, particularly deep learning, in a wide variety of issues by benefiting from advancements in hardware architecture. Advances in deep learning-based approaches, especially by taking advantage of convolutional neural networks (CNNs) in image data, have led to a significant breakthrough in a variety of computer vision tasks, including image reconstruction [27], image segmentation [28], and object classification [29]. Deep learning application in Gaussian image noise reduction has also attracted a great deal of attention as it offers vastly improved performance over classical algorithms [30–34].

Although these learning-based networks are significantly effective in removing Gaussian noise, they cannot denoise well in the presence of SAP noise, specifically at high-density noises. This poor performance of networks which are designed to remove Gaussian noise in SAP noise removal can be attributed to a variety of reasons. Firstly, these networks modify all pixels in noisy images; however, unlike Gaussian and Poissonian noise, SAP noise does not affect all pixels. Therefore, some pixels are noise-free, which should not alter throughout denoising. Needless to say, the quantity of clean pixels is considerable at low noise densities. Secondly, they restore noisy pixels using all pixels, even noisy ones, in the receptive field. In the case of SAP noise, there is no correlation between the value of noisy pixels and their original values. This phenomenon can be problematic in the denoising performance of the networks, particularly at high noise densities in which a considerable part of pixels is noisy. Thus, since SAP noise is pure noise, it can produce an adverse effect on the SAP noise removal function of CNNs [35]. Finally, since SAP is not an additive noise, a residual learning strategy, which is adopted in some of these networks such as DnCNN [30], is ineffective and introduces undesirable visual artifacts [36].

As opposed to Gaussian noise, relatively few research studies on impulse noise reduction, specifically SAP noise, use artificial neural networks (ANNs) [35, 37–39]. A non-local switching filter followed by a pretrained multi-layer perception (NLSF-MLP) model was suggested for SAP noise reduction in [37]. Fu et al. proposed employing a non-local switching filter as a preprocessing stage to a CNN (NLSF-CNN) to improve the performance of SAP noise reduction from corrupted images [35]. Since SAP can adversely affect the CNN models, the preprocessing stage is considered to prepare noisy images for the CNN model by changing the type of noise. Hence, NLSF-MLP and NLSF-CNN are indeed an integration of conventional and learning-based strategies. Moreover, NLSF-MLP and NLSF-CNN change all pixels of the images, which causes the performance to dwindle.

In spite of the fact that the approaches outlined above can be effective in SAP noise reduction, they are still suffering from a shortage of adequate performance and details preservation, especially at very high noise densities. Aiming to overcome the shortcomings of the aforementioned learning-based networks in SAP noise removal, we propose a deep convolutional neural network, namely SeConvNet, by introducing a new selective convolutional (SeConv) block. The proposed network can be extremely effective in SAP denoising, particularly at very high noise densities up to 95%, and experimental results show that it outperforms its state-of-the-art counterparts by a considerable margin in both quantitative metrics of denoising performance and visual effects.

The remainder of this paper is organized as follows. The architecture of SeConvNet and the new selective convolutional (SeConv) block are introduced in section 2. Section 3 first depicts different phases of training SeConvNet, including data employed in the training and test stages, data preprocessing, as well as network parameters and configuration. Subsequently, experimental results are reported to assess SeConvNet performance in SAP noise removal. Finally, section 4 concludes the paper.

2 The Proposed Denoising CNN Model

According to the aforementioned adverse impact of SAP noise on CNNs, we introduce a selective convolutional (SeConv) block and employ it in the first part of the proposed network model. These SeConv blocks indeed prepare the network’s input for the subsequent conventional convolutional layers and tackle the issue of participating pure noisy pixels in image reconstruction. Before proceeding to the network architecture, we first define the concept of noisy pixels map. The noisy pixels map of an arbitrary tensor \mathcal{A} is a tensor with the same shape as \mathcal{A} defined by

$$[\mathbf{M}_{\mathcal{A}}]_{i,j,k} = \begin{cases} 1 & \text{if } [\mathcal{A}]_{i,j,k} = 0 \\ 0 & \text{otherwise,} \end{cases} \quad (2)$$

where $[\mathbf{X}]_{i,j,k}$ denotes the element of \mathbf{X} at coordinates (i, j, k) . The non-noisy pixels map of \mathcal{A} , i.e., $\tilde{\mathbf{M}}_{\mathcal{A}}$, is obtained by flipping 1s and 0s in $\mathbf{M}_{\mathcal{A}}$.

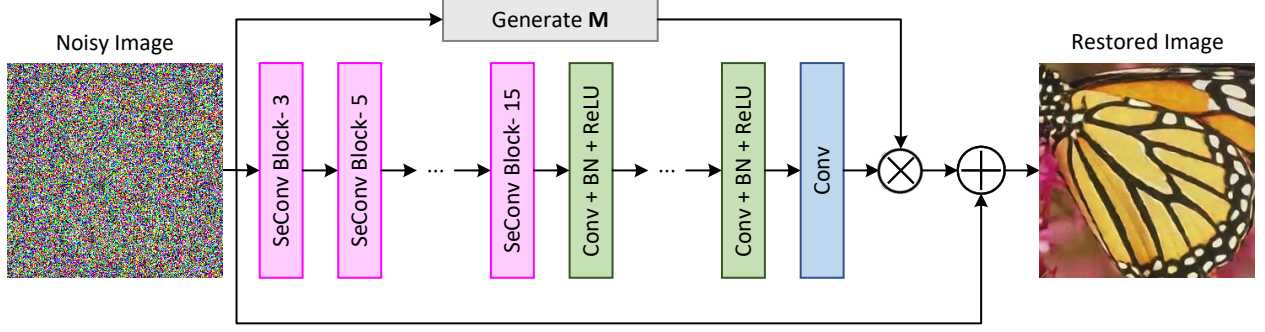


Figure 1: The architecture of SeConvNet. Note that “SeConv Block- s ” indicates a SeConv block of size s .

2.1 The Network Architecture

The architecture of the proposed SeConvNet model with D layers is shown in figure 1. The input noisy image first goes through a preprocessing stage which converts pixels with a value of 255 into 0, so that all noisy pixels will be zero thereafter. As we shall see, this will simplify the processing in the following blocks. Seven SeConv blocks constitute the first part of SeConvNet. SeConv blocks perform an initial SAP denoising and replace pure noisy pixels by an accurate estimate of them, whereby the subsequent convolutional layers could improve the denoising performance. As described in the following subsection, a SeConv block of size s selectively restores some of the noisy pixels of its input image using a trainable $s \times s$ kernel, and non-noisy pixels remain unchanged as they pass through the SeConv blocks. It should also be noted that the SeConv blocks are arranged in the ascending order of $s = 3, 5, 7, 9, 11, 13, 15$.

For the 8^{th} to $(D - 1)^{th}$ layers, convolution (Conv) with 64 filters of size 3×3 generating 64 feature maps, along with ReLU activation are used. Furthermore, to benefit from the properties of batch normalization (BN) [30], BN is considered between convolution and ReLU. In order to reconstruct images, convolution with C filters of size 3×3 is employed in the D^{th} layer, where C is the number of channels (it is equal to 1 for gray image denoising and 3 for color denoising).

Ultimately, as it is anticipated that only noisy pixels will change, the obtained output is multiplied by the noisy pixels map of the network’s input (M), and the result is then added to the input of the network to prevent any change in clean pixels.

2.2 Selective Convolutional Block

As an initial denoising step, SeConv blocks are introduced to efficiently replace pure SAP noisy pixels by a first-order estimate. To provide an efficient and accurate estimation of a SAP noisy pixel, we use a normalized weighted average of non-noisy pixels in its neighborhood [8, 40]. This weighted average filtering can be considered as a convolution between the input image \mathbb{X} and a kernel ω , in which only uncorrupted (non-noisy) pixels are used in the convolution [25], i.e.,

$$[\mathbf{S}]_{i,j,k} = \begin{cases} \frac{\sum_{l,m,n} [\mathbb{X}]_{l,m,n} [\omega]_{i-l,j-m,k-n}}{\sum_{l,m,n: [\mathbb{X}]_{l,m,n} \neq 0} [\omega]_{i-l,j-m,k-n}} & \text{if } \sum_{l,m,n: [\mathbb{X}]_{l,m,n} \neq 0} [\omega]_{i-l,j-m,k-n} \neq 0 \\ 0 & \text{otherwise.} \end{cases} \quad (3)$$

where the condition $l, m, n : [\mathbb{X}]_{l,m,n} \neq 0$ indicates that only non-noisy pixels are incorporated in the restoration process (as all noisy pixels are turned into 0 in the preprocessing stage). Using the notion of non-noisy pixels map $\tilde{M}_{\mathbb{X}}$,

we can reformulate Eq. 3 as

$$[\mathbf{S}]_{i,j,k} = \begin{cases} \frac{\sum_{l,m,n} [\mathbb{X}]_{l,m,n}[\omega]_{i-l,j-m,k-n}}{\sum_{l,m,n} [\tilde{\mathbf{M}}_{\mathbb{X}}]_{l,m,n}[\omega]_{i-l,j-m,k-n}} & \text{if } \sum_{l,m,n} [\tilde{\mathbf{M}}_{\mathbb{X}}]_{l,m,n}[\omega]_{i-l,j-m,k-n} \neq 0 \\ 0 & \text{otherwise,} \end{cases} \quad (4)$$

which can be equivalently restated as

$$[\mathbf{S}]_{i,j,k} = \begin{cases} \frac{[\mathbb{X} * \omega]_{i,j,k}}{[\tilde{\mathbf{M}}_{\mathbb{X}} * \omega]_{i,j,k}} & \text{if } [\tilde{\mathbf{M}}_{\mathbb{X}} * \omega]_{i,j,k} \neq 0 \\ 0 & \text{otherwise.} \end{cases} \quad (5)$$

where $*$ denotes the conventional convolution operation.

For weighted average filtering to effectively restore a noisy pixel, however, a sufficient number of non-noisy pixels should incorporate in the above convolution [9, 41]. Accordingly, to further improve the initial denoising, we selectively restore only those noisy pixels for which there are at least η non-noisy pixels in the local $s \times s$ around them, and the remaining noisy pixels are restored in subsequent SeConv blocks with larger kernel sizes [25]. This will assure a minimum degree of reliability for restored pixels at each block. It should also be noted that for effective denoising with weighted average filtering, the value of η should be increased with the size of the kernel (since more non-noisy pixels are required in larger windows). For a SeConv block with a size of $s \times s$, η has been set experimentally to $s - 2$. To determine the number of non-noisy pixels involved in the estimation of each noisy pixel, the non-noisy pixels map $\tilde{\mathbf{M}}_{\mathbb{X}}$ is convolved with an $s \times s$ kernel of ones (ω_{one}), and the reliability tensor is obtained as

$$[\mathbf{R}_{\mathbb{X}}]_{i,j,k} = \begin{cases} 1 & \text{if } [\tilde{\mathbf{M}}_{\mathbb{X}} * \omega_{\text{one}}]_{i,j,k} \geq \eta \\ 0 & \text{otherwise.} \end{cases} \quad (6)$$

Therefore, the non-zero entries of the element-wise product of \mathbf{S} , $\mathbf{M}_{\mathbb{X}}$, and $\mathbf{R}_{\mathbb{X}}$ yield the restored pixels which are qualified by the above reliability criterion. Noting that all noisy pixels of the input were set to zero, the restored image at the output of the SeConv block is obtained as

$$\hat{\mathbb{X}} = \mathbb{X} + \mathbf{S} \odot \mathbf{M}_{\mathbb{X}} \odot \mathbf{R}_{\mathbb{X}}. \quad (7)$$

where \odot denotes the Hadamard (element-wise) product.

The pseudo-code of the proposed SeConv block is shown in algorithm 1.

3 Experiments

3.1 Datasets

In the training stage of SeConvNet, following [42], we consider 400 images with sizes of 180×180 as the training dataset for gray-scale image denoising. To assess the SAP noise removal performance, we employ two widely used datasets in the test phase. The first dataset contains a gray-scale version of 68 natural images of sizes 321-by-481 and 481-by-321 (figure 2), which are part of the Berkeley segmentation dataset (BSD68) [43]. The second is the 20 traditional test images dataset. This dataset comprises the 512×512 gray-scale versions of “Baboon”, “Barbara”, “Blonde Woman”, “Boat”, “Bridge”, “Cameraman”, “Dark Haired Woman”, “Einstein”, “Elaine”, “Flintstones”, “Flower”, “Hill”, “House”, “Jet Plane”, “Lake”, “Lena”, “Living Room”, “Parrot”, “Peppers”, and “Pirate” images shown in figure 3.

Moreover, for color image denoising we train SeConvNet using the rest of the 500 color images in the Berkeley segmentation dataset except BSD68. We also utilized the color version of BSD68 (CBSD68) as the test data.

We choose the size of the patches for training as 40×40 by cropping the data, which is augmented by random rotation, random flip and random resizing with various scale factors of 1, 0.9, 0.8, and 0.7. We train the SeConvNet using the training dataset and its corrupted version by SAP noise with known specific noise density.

Algorithm 1: Proposed SeConv Block.

Input : \mathbb{X}, ω, η ▷ Input Image, Kernel, Minimum Reliability
Output : $\hat{\mathbb{X}}$ ▷ Output Image

```

1  $H, W \leftarrow$  Size of  $\mathbb{X}$ 
2  $C \leftarrow$  Number of Channels for  $\mathbb{X}$ 
3 for  $i \leftarrow 1$  to  $H$  do
4   for  $j \leftarrow 1$  to  $W$  do
5     for  $k \leftarrow 1$  to  $C$  do
6       if  $[\mathbb{X}]_{i,j,k} = 0$  then
7          $[\mathbf{M}_{\mathbb{X}}]_{i,j,k} \leftarrow 1$ 
8          $[\tilde{\mathbf{M}}_{\mathbb{X}}]_{i,j,k} \leftarrow 0$ 
9       else
10         $[\mathbf{M}_{\mathbb{X}}]_{i,j,k} \leftarrow 0$ 
11         $[\tilde{\mathbf{M}}_{\mathbb{X}}]_{i,j,k} \leftarrow 1$ 
12      end
13      if  $[\tilde{\mathbf{M}}_{\mathbb{X}} * \omega]_{i,j,k} \neq 0$  then
14         $[\mathbf{S}]_{i,j,k} \leftarrow \frac{[\mathbb{X} * \omega]_{i,j,k}}{[\tilde{\mathbf{M}}_{\mathbb{X}} * \omega]_{i,j,k}}$ 
15      else
16         $[\mathbf{S}]_{i,j,k} \leftarrow 0$ 
17      end
18      if  $[\tilde{\mathbf{M}}_{\mathbb{X}} * \omega]_{i,j,k} \geq \eta$  then
19         $[\mathbf{R}_{\mathbb{X}}]_{i,j,k} \leftarrow 1$ 
20      else
21         $[\mathbf{R}_{\mathbb{X}}]_{i,j,k} \leftarrow 0$ 
22      end
23    end
24  end
25 end
26  $\hat{\mathbb{X}} \leftarrow \mathbb{X} + \mathbf{M}_{\mathbb{X}} \mathbf{R}_{\mathbb{X}} \mathbf{S}$ 

```

3.2 Preprocessing Stage

As a preprocessing step, all noisy pixels are set to zero before feeding to SeConvNet. The process can be easily accomplished by converting all pixels with values of 255 to 0. The principal reason is to make all noisy pixels numerically identical.

3.3 Network Training

To meet the need for enough spatial information in the noise reduction task and also to consider the complexity of the network, we set the network depth D to 27. We utilize ones and orthogonal matrices as the initial weights of the SeConv blocks and convolutions, respectively. Moreover, all biases are set to zero during the training stage. The following loss function is adopted to train the trainable parameters of the network Θ for predicting the clean images using P patches

$$\mathcal{L}(\Theta) = \frac{1}{2P} \sum_{i=1}^P \|\mathcal{F}(\mathbf{X}_i; \Theta) - \mathbf{Y}_i\|^2. \quad (8)$$



Figure 2: The BSD68 dataset.

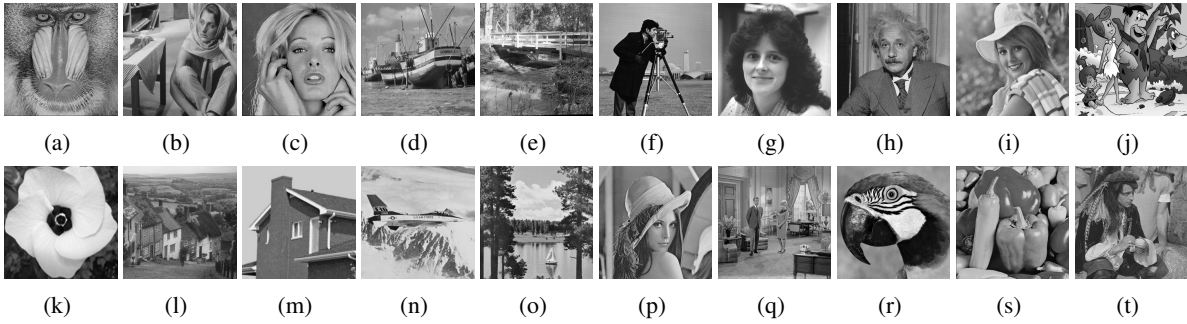


Figure 3: The 20 traditional test images dataset. (a) Baboon (b) Barbara (c) Blonde Woman (d) Boat (e) Bridge (f) Cameraman (g) Dark Haired Woman (h) Einstein (i) Elaine (j) Flintstones (k) Flower (l) Hill (m) House (n) Jet Plane (o) Lake (p) Lena (q) Living Room (r) Parrot (s) Peppers (t) Pirate.

where $\hat{\mathbf{X}} = \mathcal{F}(\mathbf{X}; \Theta)$ is the estimated image from the input noisy observation \mathbf{X} , and \mathbf{Y} is the desired clean image. The loss function is minimized using the ADAM solver algorithm [44] with α of $1e-3$, β_1 of 0.9, β_2 of 0.999, and ϵ of $1e-7$. The network is trained 50 epochs with a batch size of 128. The learning rate declines from $1e-3$ to $1e-4$. The model was trained in the Python Programming Language using the TensorFlow library running on a 64-bit operating system with an Intel® Core™ i9-9900K processor, 64GB of RAM, and an NVIDIA GeForce RTX 2070 graphics card.

3.4 Evaluation Criteria

Peak signal-to-noise ratio (PSNR) is widely used to measure the performance of different denoising approaches. A higher PSNR value indicates that the denoised image, in general, is closer to the original image and has a higher visual quality. In addition, the structural similarity index measure (SSIM) criterion [45] is utilized as well, since PSNR would yield unreliable results in some cases [46]. SSIM is a measurement of structural similarity between two images, and its value ranges between 0 and 1. The higher the SSIM value, the more structural similarity.

For an original (desired clean) image \mathbf{Y} and its denoised image $\hat{\mathbf{X}}$ of size $H \times W$ and C channels, PSNR (dB) is defined as

$$\text{PSNR}(\hat{\mathbf{X}}, \mathbf{Y}) = 10 \log_{10} \left(\frac{255^2}{\text{MSE}(\hat{\mathbf{X}}, \mathbf{Y})} \right), \quad (9)$$

where

$$\text{MSE}(\hat{\mathbf{X}}, \mathbf{Y}) = \frac{1}{CHW} \sum_{k=1}^C \sum_{i=1}^H \sum_{j=1}^W (\hat{\mathbf{X}}_{i,j,k} - \mathbf{Y}_{i,j,k})^2 \quad (10)$$

Table 1: Results of PSNR (dB) for different methods at different noise densities on the 20 traditional test images and BSD68 gray-scale datasets.

Dataset	Methods	10%	20%	30%	40%	50%	60%	70%	80%	90%	95%	Mean
20TTI	ADKIF	40.64	37.63	35.61	33.86	32.12	30.30	28.47	26.66	24.68	23.09	31.31
	NLSF-MLP	38.95	34.74	31.95	29.79	27.96	26.24	26.62	24.25	20.85	19.51	28.09
	NLSF-CNN	40.39	36.03	33.13	31.67	29.72	27.89	27.29	24.87	21.38	20.00	29.24
	ARmF	41.29	38.10	35.98	34.20	32.54	30.89	29.20	27.34	24.83	22.90	31.73
	ACmF	40.93	37.80	35.72	34.00	32.40	30.82	29.19	27.39	24.92	22.89	31.61
	IAWMF	41.39	38.26	36.17	34.43	32.81	31.20	29.61	27.96	25.57	23.54	32.09
	NAHAT	42.22	38.94	36.72	34.90	33.27	31.69	30.04	28.17	25.70	23.85	32.55
	DAMRmF	41.36	38.23	36.14	34.40	32.82	31.21	29.63	27.97	25.57	23.42	32.07
	SeConvNet	44.30	41.28	39.53	36.45	35.85	34.92	32.85	31.14	28.29	25.88	35.05
BSD68	ADKIF	36.72	33.63	31.68	30.12	28.65	27.17	25.69	24.24	22.68	21.48	28.21
	NLSF-MLP	35.20	31.05	28.43	26.50	24.94	23.54	24.02	22.05	19.16	18.14	25.30
	NLSF-CNN	36.50	32.20	29.48	28.17	26.51	25.02	24.63	22.61	19.65	18.61	26.34
	ARmF	36.76	33.56	31.54	29.93	28.47	27.06	25.61	24.05	22.04	20.52	27.95
	ACmF	36.22	33.05	31.09	29.55	28.18	26.84	25.47	23.96	22.03	20.51	27.69
	IAWMF	37.26	34.19	32.21	30.61	29.17	27.82	26.43	24.93	22.98	21.50	28.71
	NAHAT	38.35	34.96	32.77	31.07	29.60	28.24	26.90	25.46	23.67	22.30	29.33
	DAMRmF	36.05	32.87	30.87	29.33	27.98	26.73	25.50	24.17	22.40	20.84	27.67
	SeConvNet	40.47	37.36	35.13	33.12	30.36	30.41	28.67	27.23	24.83	23.21	31.08

is the mean square error (MSE) between $\hat{\mathbf{X}}$ and \mathbf{Y} , and SSIM is defined as

$$\text{SSIM}(\hat{\mathbf{X}}, \mathbf{Y}) = \frac{(2\mu_{\hat{\mathbf{X}}}\mu_{\mathbf{Y}} + c_1)(2\sigma_{\hat{\mathbf{X}}\mathbf{Y}} + c_2)}{(\mu_{\hat{\mathbf{X}}}^2 + \mu_{\mathbf{Y}}^2 + c_1)(\sigma_{\hat{\mathbf{X}}}^2 + \sigma_{\mathbf{Y}}^2 + c_2)}. \quad (11)$$

Here $\mu_{\hat{\mathbf{X}}}$, $\mu_{\mathbf{Y}}$, $\sigma_{\hat{\mathbf{X}}}$, $\sigma_{\mathbf{Y}}$, and $\sigma_{\hat{\mathbf{X}}\mathbf{Y}}$ indicate, respectively, the average intensity of $\hat{\mathbf{X}}$, average intensity of \mathbf{Y} , standard deviation of $\hat{\mathbf{X}}$, standard deviation of \mathbf{Y} , and cross-covariance of $\hat{\mathbf{X}}$ and \mathbf{Y} . The two small constants $c_1 = (k_1L)^2$ and $c_2 = (k_2L)^2$ are used for division stabilization. The value of L is assumed to be 255 for 8-bit gray-scale version of images and the default values of k_1 , k_2 are considered to be 0.01 and 0.03.

3.5 Experiments on SAP noise Removal

In this subsection, we discuss the results of SAP denoising measured by PSNR and SSIM. A comparison is provided between the proposed SeConvNet and seven state-of-the-art methods, including ADKIF [9], NLSF-MLP [37], NLSF-CNN [35], ARmF [21], ACmF [23], IAWMF [20], NAHAT [26], and DAMRmF [22]. The source code of SeConvNet is available at <https://github.com/AliRafiee7/SeConvNet>.

Tables 1 to 4 report the SAP denoising performance of the proposed SeConvNet as well as the state-of-the-art competing methods based on the PSNR (dB) and SSIM criteria at varying noise densities ranging from 10% to 95%. In addition, the average performance results of 10% to 95% noise densities are presented in the last column of the tables. The best result of each noise density is highlighted in bold font. Table 1 contains the PSNR (dB) results of gray-scale SAP noise

Table 2: Results of PSNR (dB) for different methods at different noise densities on the CBSD68 color dataset.

Dataset	Methods	10%	20%	30%	40%	50%	60%	70%	80%	90%	95%	Mean
CBSD68	ADKIF	34.53	32.24	30.63	29.26	27.95	26.60	25.25	23.89	22.40	21.21	27.40
	NLSF-MLP	33.10	29.77	27.48	25.75	24.33	23.04	23.61	21.74	18.93	17.92	24.57
	NLSF-CNN	34.32	30.87	28.50	27.37	25.86	24.49	24.21	22.29	19.41	18.38	25.57
	ARmF	35.11	32.62	30.87	29.42	28.07	26.74	25.37	23.85	21.90	20.38	27.43
	ACmF	34.63	32.15	30.46	29.07	27.79	26.53	25.23	23.78	21.88	20.38	27.19
	IAWMF	35.19	32.95	31.30	29.89	28.61	27.35	26.06	24.62	22.73	21.26	28.00
	NAHAT	36.63	33.97	32.08	30.54	29.18	27.90	26.62	25.23	23.47	22.10	28.77
	DAMRmF	33.92	31.49	29.85	28.56	27.40	26.29	25.18	23.93	22.21	20.62	26.94
	SeConvNet	45.10	42.64	39.70	38.19	34.87	33.82	32.20	29.82	26.64	24.38	34.73

Table 3: Results of SSIM for different methods at different noise densities on the 20 traditional test images and BSD68 gray-scale datasets.

Dataset	Methods	10%	20%	30%	40%	50%	60%	70%	80%	90%	95%	Mean
20TTI	ADKIF	0.987	0.973	0.958	0.940	0.916	0.883	0.836	0.772	0.685	0.616	0.857
	NLSF-MLP	0.946	0.899	0.860	0.827	0.798	0.765	0.782	0.702	0.579	0.521	0.768
	NLSF-CNN	0.981	0.932	0.892	0.879	0.848	0.813	0.802	0.720	0.593	0.534	0.799
	ARmF	0.988	0.976	0.962	0.945	0.924	0.897	0.861	0.810	0.725	0.647	0.873
	ACmF	0.987	0.974	0.959	0.942	0.921	0.893	0.857	0.807	0.723	0.645	0.871
	IAWMF	0.988	0.976	0.962	0.945	0.924	0.897	0.862	0.812	0.743	0.672	0.878
	NAHAT	0.989	0.977	0.964	0.948	0.928	0.904	0.871	0.824	0.746	0.677	0.883
	DAMRmF	0.988	0.976	0.961	0.945	0.924	0.897	0.862	0.813	0.744	0.671	0.878
	SeConvNet	0.995	0.991	0.986	0.975	0.972	0.963	0.948	0.927	0.882	0.833	0.947
BSD68	ADKIF	0.983	0.964	0.943	0.918	0.886	0.841	0.780	0.700	0.597	0.524	0.814
	NLSF-MLP	0.942	0.890	0.846	0.808	0.771	0.729	0.729	0.637	0.504	0.443	0.730
	NLSF-CNN	0.977	0.923	0.877	0.859	0.820	0.774	0.748	0.653	0.517	0.454	0.760
	ARmF	0.983	0.966	0.948	0.925	0.897	0.861	0.813	0.747	0.643	0.555	0.834
	ACmF	0.981	0.963	0.942	0.918	0.889	0.853	0.806	0.741	0.639	0.553	0.829
	IAWMF	0.986	0.970	0.952	0.930	0.903	0.869	0.824	0.763	0.664	0.582	0.844
	NAHAT	0.988	0.973	0.955	0.932	0.905	0.870	0.824	0.761	0.665	0.588	0.846
	DAMRmF	0.975	0.958	0.939	0.917	0.890	0.857	0.813	0.754	0.659	0.574	0.834
	SeConvNet	0.993	0.987	0.979	0.966	0.946	0.936	0.907	0.875	0.804	0.742	0.913

reduction on the 20 traditional test images and BSD68 datasets. The PSNR results of color SAP denoising on CBSD68 are listed in table 2. Also included in tables 3 and 4 are the SSIM results of gray-scale and color SAP denoising.

As one can see in the results of the 20 traditional test images, BSD68, and CBSD68 datasets, SeConvNet can attain the best PSNR/SSIM results compared to other counterparts at low, moderate, and high noise densities. SeConvNet surpasses NAHAT, which has the second-best PSNR/SSIM results, by a significant margin. On average, SeConvNet outperforms NAHAT by 2.5dB/0.064, 1.7dB/0.067, and 6.0dB/0.045 in the PSNR/SSIM criterion on the 20 traditional

Table 4: Results of SSIM for different methods at different noise densities on CBSD68 color dataset.

Dataset	Methods	10%	20%	30%	40%	50%	60%	70%	80%	90%	95%	Mean
CBSD68	ADKIF	0.984	0.973	0.960	0.944	0.924	0.897	0.859	0.809	0.741	0.685	0.878
	NLSF-MLP	0.944	0.898	0.861	0.831	0.804	0.777	0.803	0.736	0.626	0.579	0.786
	NLSF-CNN	0.978	0.931	0.893	0.883	0.855	0.825	0.824	0.755	0.642	0.594	0.818
	ARmF	0.985	0.975	0.964	0.950	0.933	0.910	0.879	0.836	0.762	0.692	0.889
	ACmF	0.984	0.973	0.960	0.946	0.928	0.905	0.875	0.832	0.760	0.692	0.885
	IAWMF	0.987	0.978	0.967	0.953	0.936	0.915	0.887	0.846	0.777	0.713	0.896
	NAHAT	0.990	0.981	0.970	0.956	0.940	0.919	0.891	0.852	0.789	0.735	0.902
	DAMRmF	0.970	0.959	0.948	0.935	0.920	0.900	0.875	0.838	0.773	0.705	0.882
	SeConvNet	0.997	0.995	0.992	0.989	0.976	0.971	0.959	0.932	0.869	0.794	0.947

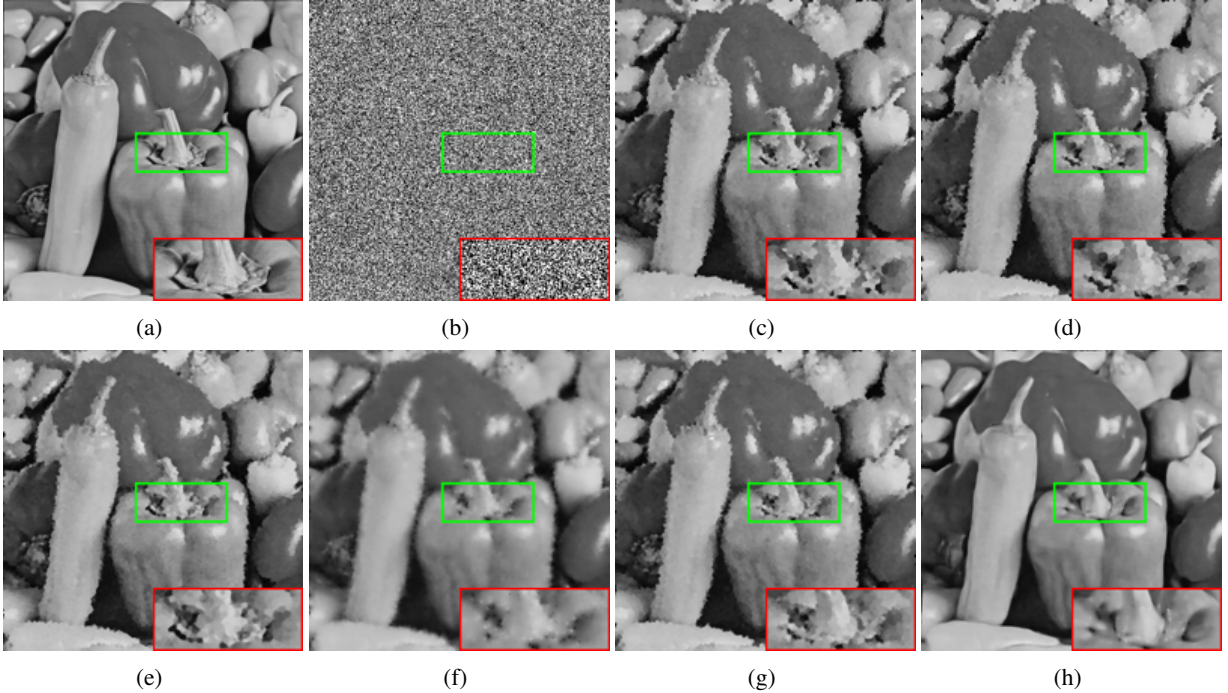


Figure 4: Restoration results of different methods for the Peppers image with 95% SAP noise. (a) Original image (b) Noisy image (c) ARmF (d) ACmF (e) IAWMF (f) NAHAT (g) DAMRmF (h) SeConvNet.

test images, BSD68, and CBSD68 datasets, respectively. Specifically, at very high noise density, i.e., 95%, while NAHAT can denoise the images in the 20 traditional test images, BSD68, and CBSD68 datasets with a PSNR/SSIM performance of about 23.8dB/0.883, 22.3dB/0.846, 22.10dB/0.735, SeConvNet can drastically boost PSNR/SSIM gain on these datasets to 25.8dB/0.947, 23.2dB/0.913, and 24.38dB/0.794. Aside from SeConvNet and NAHAT, IAWMF can offer the best performance among other remaining methods on these datasets.

To show the SAP denoising efficiency of SeConvNet at a very high noise density, we choose three gray and three color images and illustrate the visual results of various methods on the corrupted version of them by 95% SAP noise in Figures 4 to 9. Based on the results shown, it is evident that ARmF, ACmF, IAWMF, and DAMRmF fail to recover the edges and details and produce artifacts in the edges. The NAHAT method blurs images and generates overly smooth

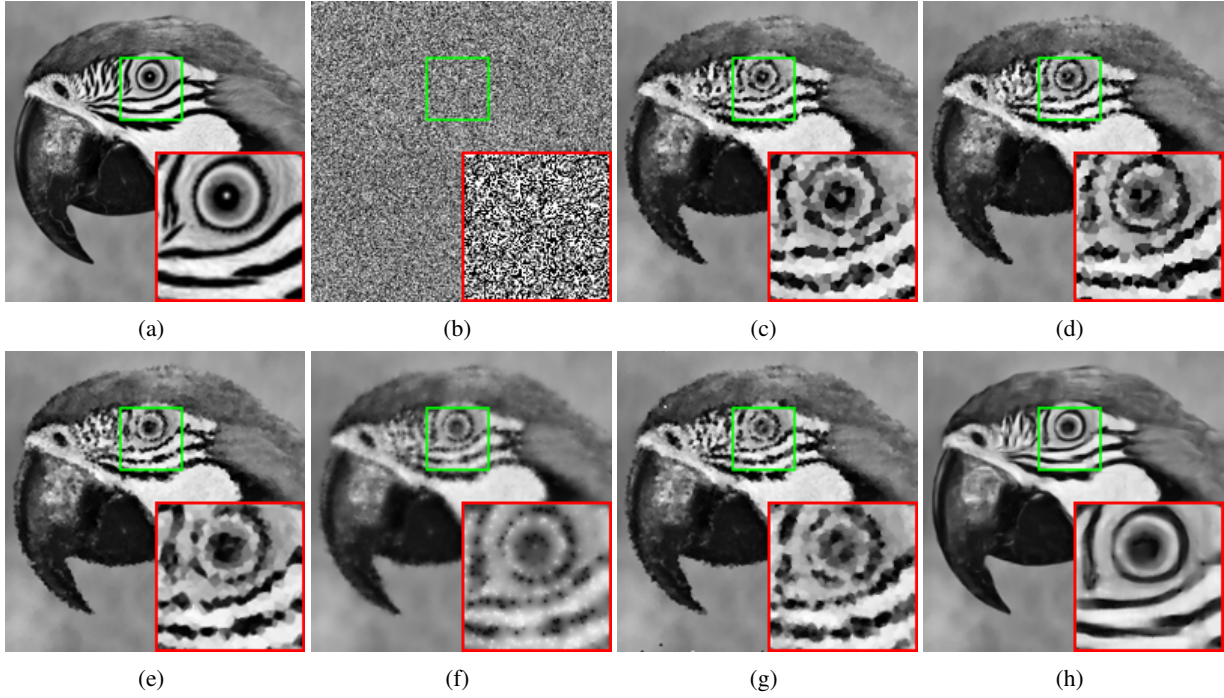


Figure 5: Restoration results of different methods for the Parrot image with 95% SAP noise. (a) Original image (b) Noisy image (c) ARmF (d) ACmF (e) IAWMF (f) NAHAT (g) DAMRmF (h) SeConvNet.

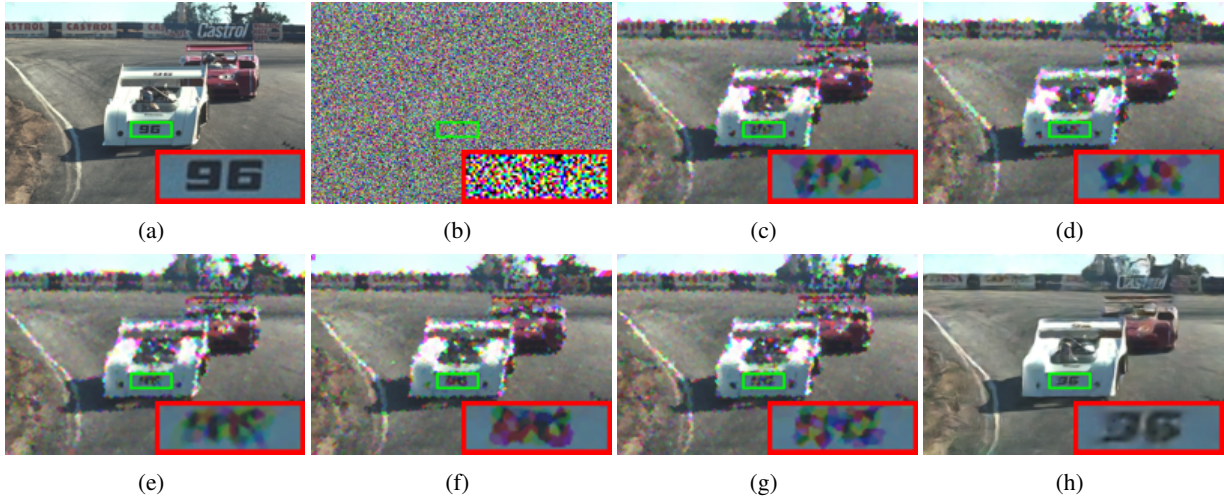


Figure 6: Restoration results of different methods for one image from the CBSD68 dataset with 95% SAP noise. (a) Original image (b) Noisy image (c) ARmF (d) ACmF (e) IAWMF (f) NAHAT (g) DAMRmF (h) SeConvNet.

textures and edges. However, SeConvNet not only preserves fine details and sharp edges but also provides impressive visual results in smooth regions. For instance, it is obviously seen that while other methods fail to recover the eye and the surrounding area of the parrot’s eye in figure 5, SeConvNet can effectively preserve fine details and sharp edges, as well as textures. Also, in figure 6 the number 96 on the white racing car becomes entirely indistinct by other SAP denoising methods, whereas it is almost clearly visible by SeConvNet. Moreover, in the case of color SAP denoising, ARmF, ACmF, IAWMF, NAHAT, and DAMRmF tend to introduce false color artifacts in addition to losing edges and

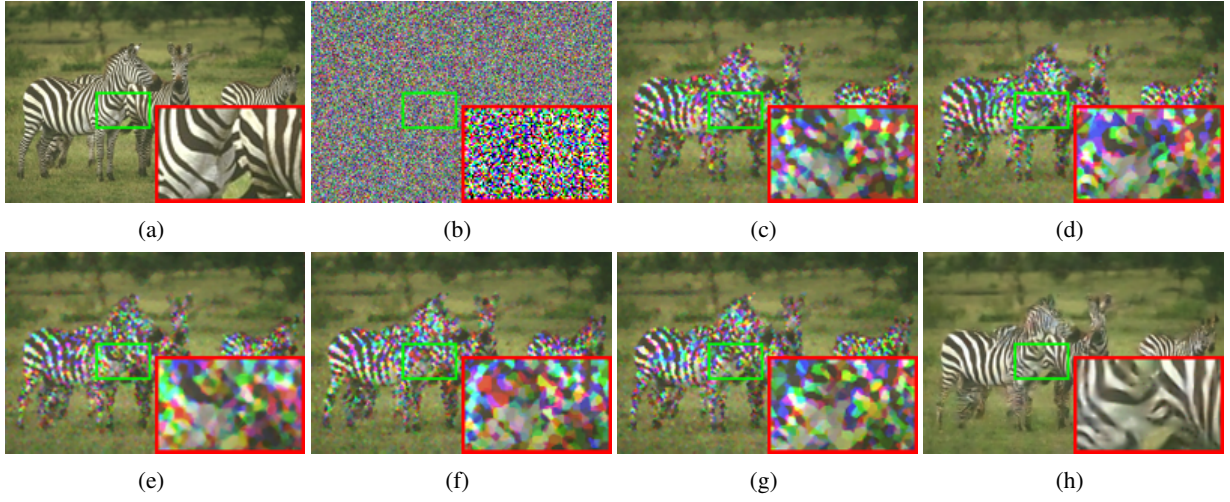


Figure 7: Restoration results of different methods for one image from the CBSD68 dataset with 95% SAP noise. (a) Original image (b) Noisy image (c) ARmF (d) ACmF (e) IAWMF (f) NAHAT (g) DAMRmF (h) SeConvNet.

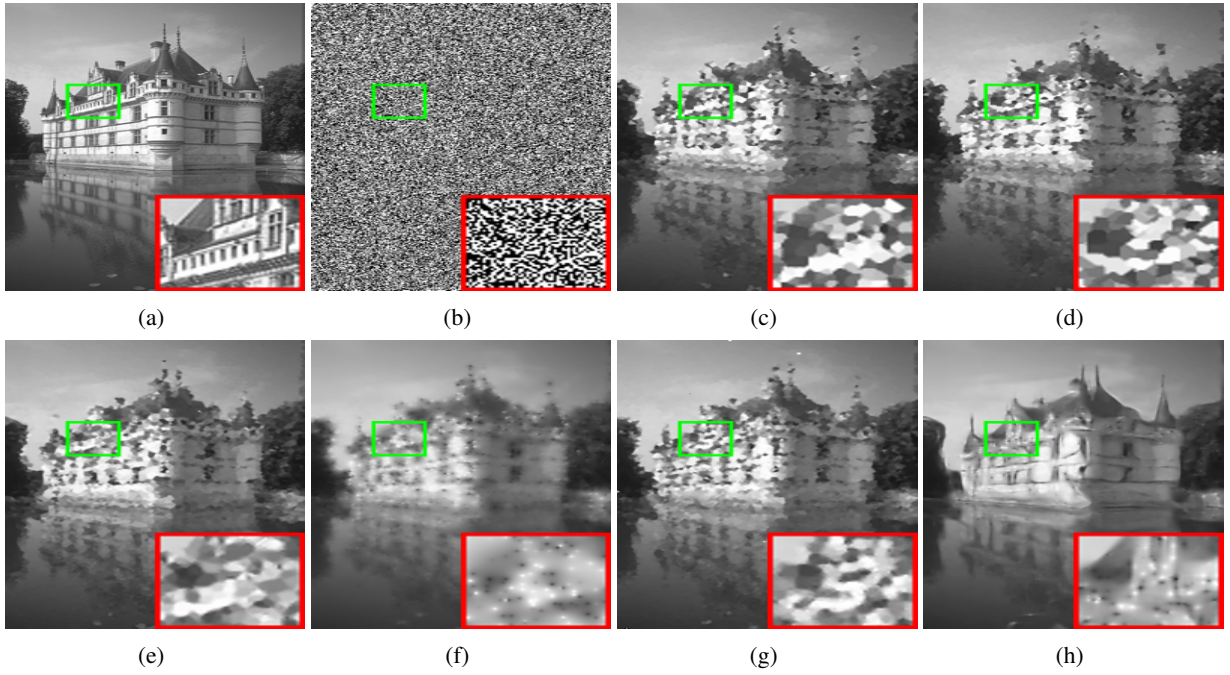


Figure 8: Restoration results of different methods for one image from the BSD68 dataset with 95% SAP noise. (a) Original image (b) Noisy image (c) ARmF (d) ACmF (e) IAWMF (f) NAHAT (g) DAMRmF (h) SeConvNet.

details. These false-color artifacts are clearly apparent in figure 7, whilst SeConvNet can recover high-quality visual results without any false-color artifacts.

For better visual comparison of the obtained results, figures 10, 11, and 12 demonstrate the line graph of the average PSNR (dB) and SSIM versus noise densities for the 20 traditional test images, BSD68, and CBSD68 dataset, respectively. As it can be obviously seen, the proposed SeConvNet model can consistently surpass other state-of-the-art methods by a considerable margin.

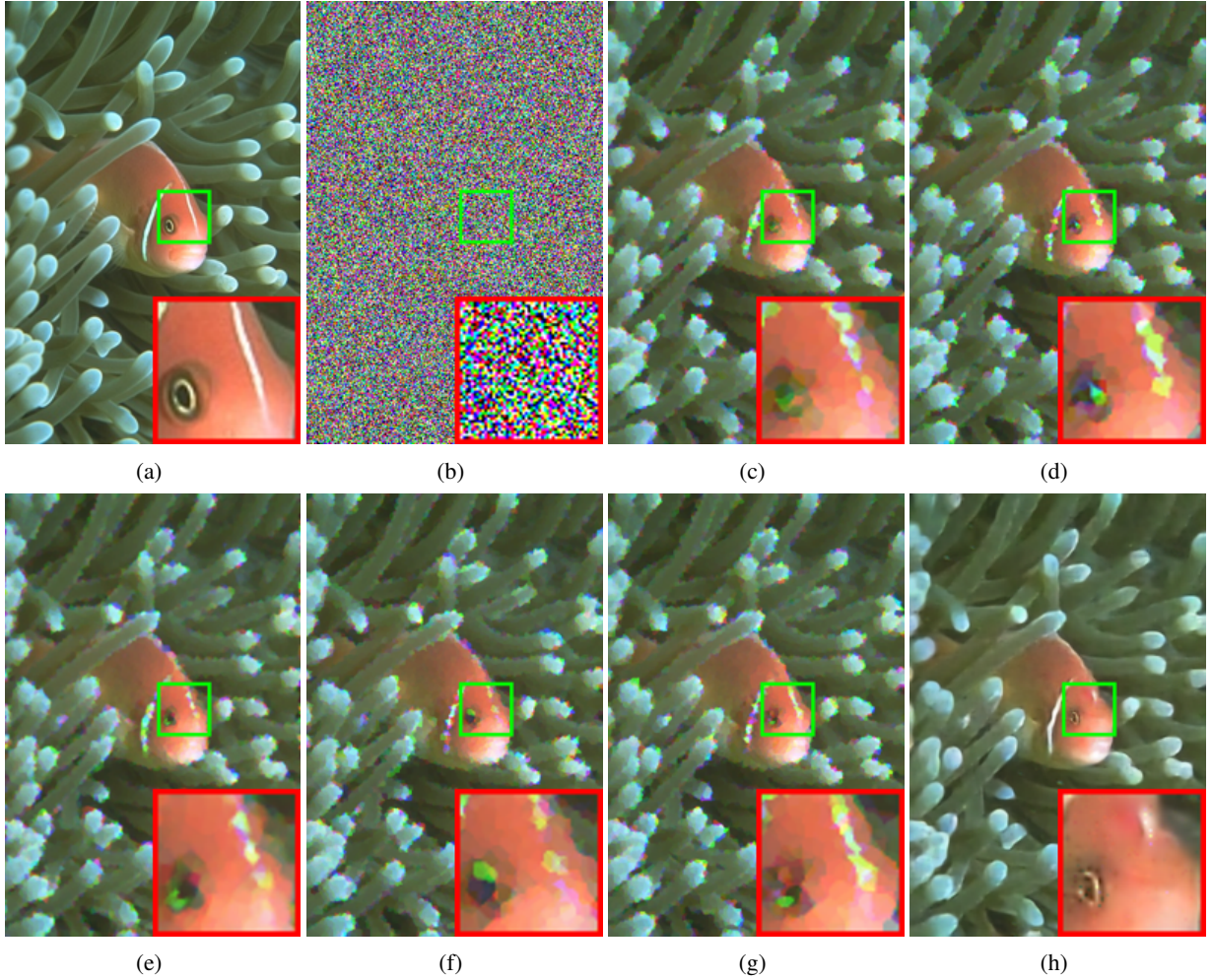


Figure 9: Restoration results of different methods for one image from the CBSD68 dataset with 95% SAP noise. (a) Original image (b) Noisy image (c) ARmF (d) ACmF (e) IAWMF (f) NAHAT (g) DAMRmF (h) SeConvNet.

4 Conclusion

A new CNN model, namely SeConvNet, is proposed in this paper to denoise both gray-scale and color images corrupted by SAP noise, especially at high and very high noise densities. To meet this purpose, we introduced a new selective convolutional (SeConv) block for the beginning part of the network, which computes an initial estimation of noisy pixels by considering only non-noisy pixels. In the following layers of the network, conventional convolutional layers, as well as batch normalization (BN) and rectified linear units (ReLU), are employed. The denoising performance of SeConvNet is compared with seven state-of-the-art methods in terms of the PSNR and SSIM criteria on different gray-scale and color datasets, including 20 traditional test images and gray and color versions of 68 images of the Berkeley segmentation dataset (BSD68 and CBSD68). The results indicate that SeConvNet not only surpasses all counterparts by a significant margin (particularly at high noise densities) in quantitative denoising performance but also produces favorable restored images by preserving fine details and sharp edges along with providing impressive visual results in the smooth region.

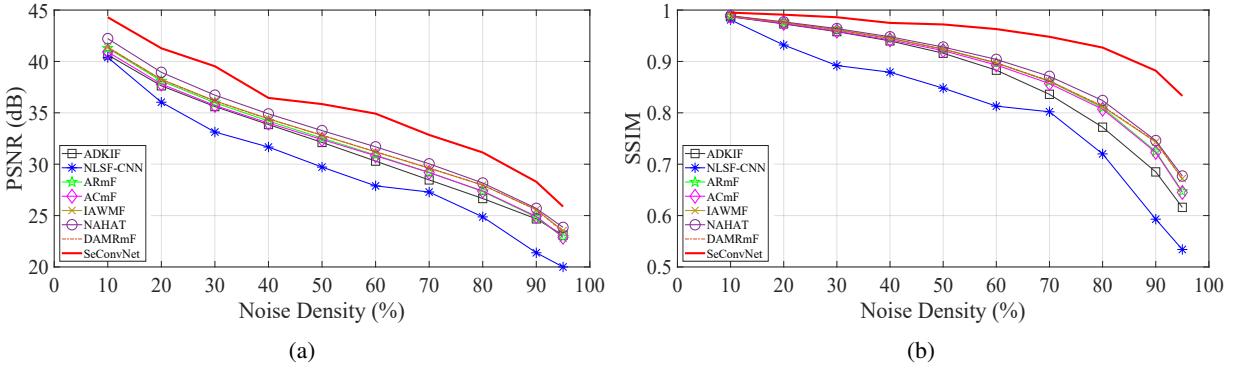


Figure 10: Comparison graphs of the averages of different metrics on the 20 traditional test images dataset versus different noise densities. (a) PSNR (dB) (b) SSIM.

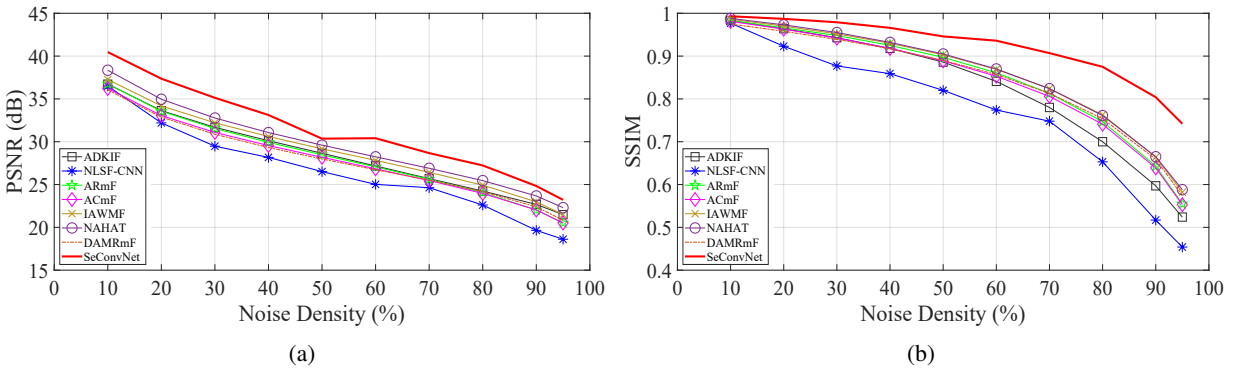


Figure 11: Comparison graphs of the averages of different metrics on the BSD68 dataset versus different noise densities. (a) PSNR (dB) (b) SSIM.

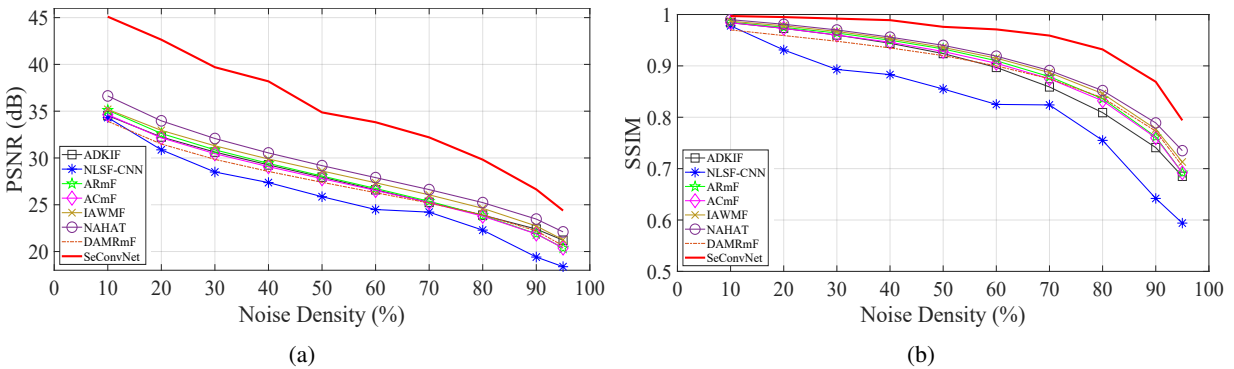


Figure 12: Comparison graphs of the averages of different metrics on the CBSD68 dataset versus different noise densities. (a) PSNR (dB) (b) SSIM.

References

- [1] Alan C Bovik. *Handbook of Image and Video Processing*. Communications, Networking and Multimedia. Academic Press Inc, 2nd edition, 2005. ISBN 9780080533612. doi:<https://doi.org/10.1016/B978-0-12-119792-6.X5062-1>.

- [2] Vivek Singh Bhadouria, Dibyendu Ghoshal, and Abul Hasan Siddiqi. A new approach for high density saturated impulse noise removal using decision-based coupled window median filter. *Signal, Image and Video Processing*, 8(1):71–84, Jan 2014. ISSN 1863-1711. doi:<https://doi.org/10.1007/s11760-013-0487-5>.
- [3] G. Ghimpeanu, T. Batard, M. Bertalmío, and S. Levine. A decomposition framework for image denoising algorithms. *IEEE Transactions on Image Processing*, 25(1):388–399, 2016. doi:<https://doi.org/10.1109/TIP.2015.2498413>.
- [4] Shaoping Xu, Xiaohui Yang, and Shunliang Jiang. A fast nonlocally centralized sparse representation algorithm for image denoising. *Signal Processing*, 131:99–112, 2017. ISSN 0165-1684. doi:<https://doi.org/10.1016/j.sigpro.2016.08.006>.
- [5] Rafael C. Gonzalez and Richard E. Woods. *Digital Image Processing*. Pearson Education, 4th edition, 2018. ISBN 9781292223049.
- [6] Jaakko Astola and Pauli Kuosmanen. *Fundamentals of Nonlinear Digital Filtering*, volume 8. CRC press, 1997. ISBN 0849325706.
- [7] S. Esakkirajan, T. Veerakumar, A. N. Subramanyam, and C. H. PremChand. Removal of high density salt and pepper noise through modified decision based unsymmetric trimmed median filter. *IEEE Signal Processing Letters*, 18(5):287–290, 2011. doi:<https://doi.org/10.1109/LSP.2011.2122333>.
- [8] P. Zhang and F. Li. A new adaptive weighted mean filter for removing salt-and-pepper noise. *IEEE Signal Processing Letters*, 21(10):1280–1283, 2014. doi:<https://doi.org/10.1109/LSP.2014.2333012>.
- [9] R. Varatharajan, K. Vasanth, M. Gunasekaran, M. Priyan, and X.Z. Gao. An adaptive decision based kriging interpolation algorithm for the removal of high density salt and pepper noise in images. *Computers & Electrical Engineering*, 70:447–461, 2018. ISSN 0045-7906. doi:<https://doi.org/10.1016/j.compeleceng.2017.05.035>.
- [10] Ugur Erkan, Levent Gökrem, and Serdar Enginoglu. Different applied median filter in salt and pepper noise. *Computers & Electrical Engineering*, 70:789–798, 2018. ISSN 0045-7906. doi:<https://doi.org/10.1016/j.compeleceng.2018.01.019>.
- [11] K. Vasanth and R. Varatharajan. An adaptive content based closer proximity pixel replacement algorithm for high density salt and pepper noise removal in images. *Journal of Ambient Intelligence and Humanized Computing*, Jul 2020. ISSN 1868-5145. doi:<https://doi.org/10.1007/s12652-020-02376-2>.
- [12] B. Karthik, T. Krishna Kumar, S. P. Vijayaragavan, and M. Sriram. Removal of high density salt and pepper noise in color image through modified cascaded filter. *Journal of Ambient Intelligence and Humanized Computing*, 12(3):3901–3908, Mar 2021. ISSN 1868-5145. doi:<https://doi.org/10.1007/s12652-020-01737-1>.
- [13] Amarjit Roy and Rabul Hussain Laskar. Multiclass svm based adaptive filter for removal of high density impulse noise from color images. *Applied Soft Computing*, 46:816–826, 2016. ISSN 1568-4946. doi:<https://doi.org/10.1016/j.asoc.2015.09.032>.
- [14] Manuel González-Hidalgo, Sebastia Massanet, Arnau Mir, and Daniel Ruiz-Aguilera. Improving salt and pepper noise removal using a fuzzy mathematical morphology-based filter. *Applied Soft Computing*, 63:167–180, 2018. ISSN 1568-4946. doi:<https://doi.org/10.1016/j.asoc.2017.11.030>.
- [15] H. Hwang and R. A. Haddad. Adaptive median filters: new algorithms and results. *IEEE Transactions on Image Processing*, 4(4):499–502, 1995. doi:<https://doi.org/10.1109/83.370679>.
- [16] K. S. Srinivasan and D. Ebenezer. A new fast and efficient decision-based algorithm for removal of high-density impulse noises. *IEEE Signal Processing Letters*, 14(3):189–192, 2007. doi:<https://doi.org/10.1109/LSP.2006.884018>.

- [17] V. Jayaraj and D. Ebenezer. A new switching-based median filtering scheme and algorithm for removal of high-density salt and pepper noise in images. *EURASIP Journal on Advances in Signal Processing*, page 690218, Jul 2010. ISSN 1687-6180. doi:<https://doi.org/10.1155/2010/690218>.
- [18] A. Bovik. Streaking in median filtered images. *IEEE Transactions on Acoustics, Speech, and Signal Processing*, 35(4):493–503, 1987. doi:<https://doi.org/10.1109/TASSP.1987.1165153>.
- [19] Dang N.H. Thanh, Nguyen Ngoc Hien, P. Kalavathi, and V.B. Surya Prasath. Adaptive switching weight mean filter for salt and pepper image denoising. *Procedia Computer Science*, 171:292–301, 2020. ISSN 1877-0509. doi:<https://doi.org/10.1016/j.procs.2020.04.031>. Third International Conference on Computing and Network Communications (CoCoNet’19).
- [20] Uğur Erkan, Dang NH Thanh, Serdar Enginoğlu, and Samet Memiş. Improved adaptive weighted mean filter for salt-and-pepper noise removal. In *2020 International Conference on Electrical, Communication, and Computer Engineering (ICECCE)*, pages 1–5, 2020. doi:<https://doi.org/10.1109/ICECCE49384.2020.9179351>.
- [21] Serdar Enginoğlu, Uğur Erkan, and Samet Memiş. Pixel similarity-based adaptive riesz mean filter for salt-and-pepper noise removal. *Multimedia Tools and Applications*, 78(24):35401–35418, Dec 2019. ISSN 1573-7721. doi:<https://doi.org/10.1007/s11042-019-08110-1>.
- [22] Samet Memiş and Uğur Erkan. Different adaptive modified riesz mean filter for high-density salt-and-pepper noise removal in grayscale images. *Avrupa Bilim ve Teknoloji Dergisi*, pages 359 – 367, 2021. doi:<https://doi.org/10.31590/ejosat.873312>.
- [23] Serdar Enginoğlu, Uğur Erkan, and Samet Memiş. Adaptive cesáro mean filter for salt-and-pepper noise removal. *El-Cezeri Journal of Science and Engineering*, 7(1):304–314, 2020. doi:<https://doi.org/10.31202/ecjse.646359>.
- [24] Bharat Garg and K. V. Arya. Four stage median-average filter for healing high density salt and pepper noise corrupted images. *Multimedia Tools and Applications*, 79(43):32305–32329, Nov 2020. ISSN 1573-7721. doi:<https://doi.org/10.1007/s11042-020-09557-3>.
- [25] Ahmad Ali Rafiee and Mahmoud Farhang. A very fast and efficient multistage selective convolution filter for removal of salt and pepper noise. *Journal of Ambient Intelligence and Humanized Computing*, Mar 2022. ISSN 1868-5145. doi:<https://doi.org/10.1007/s12652-022-03747-7>.
- [26] Dang N.H. Thanh, V.B.Surya Prasath, Thai Kim Phung, and Nguyen Quoc Hung. Impulse denoising based on noise accumulation and harmonic analysis techniques. *Optik*, 241:166163, 2021. ISSN 0030-4026. doi:<https://doi.org/10.1016/j.ijleo.2020.166163>.
- [27] Chunwei Tian, Lunke Fei, Wenxian Zheng, Yong Xu, Wangmeng Zuo, and Chia-Wen Lin. Deep learning on image denoising: An overview. *Neural Networks*, 131:251–275, 2020. ISSN 0893-6080. doi:<https://doi.org/10.1016/j.neunet.2020.07.025>.
- [28] Shervin Minaee, Yuri Boykov, Fatih Porikli, Antonio Plaza, Nasser Kehtarnavaz, and Demetri Terzopoulos. Image segmentation using deep learning: A survey. *IEEE Transactions on Pattern Analysis and Machine Intelligence*, 44(7):3523–3542, 2022. doi:<https://doi.org/10.1109/TPAMI.2021.3059968>.
- [29] Li Liu, Wanli Ouyang, Xiaogang Wang, Paul Fieguth, Jie Chen, Xinwang Liu, and Matti Pietikäinen. Deep learning for generic object detection: A survey. *International Journal of Computer Vision*, 128(2):261–318, Feb 2020. ISSN 1573-1405. doi:<https://doi.org/10.1007/s11263-019-01247-4>.
- [30] Kai Zhang, Wangmeng Zuo, Yunjin Chen, Deyu Meng, and Lei Zhang. Beyond a gaussian denoiser: Residual learning of deep cnn for image denoising. *IEEE Transactions on Image Processing*, 26(7):3142–3155, 2017. doi:<https://doi.org/10.1109/TIP.2017.2662206>.

- [31] Kai Zhang, Wangmeng Zuo, and Lei Zhang. Ffdnet: Toward a fast and flexible solution for cnn-based image denoising. *IEEE Transactions on Image Processing*, 27(9):4608–4622, 2018. doi:<https://doi.org/10.1109/TIP.2018.2839891>.
- [32] Diego Valsesia, Giulia Fracastoro, and Enrico Magli. Deep graph-convolutional image denoising. *IEEE Transactions on Image Processing*, 29:8226–8237, 2020. doi:<https://doi.org/10.1109/TIP.2020.3013166>.
- [33] Kai Zhang, Yawei Li, Wangmeng Zuo, Lei Zhang, Luc Van Gool, and Radu Timofte. Plug-and-play image restoration with deep denoiser prior. *IEEE Transactions on Pattern Analysis and Machine Intelligence*, pages 1–1, 2021. doi:<https://doi.org/10.1109/TPAMI.2021.3088914>.
- [34] Yulun Zhang, Yapeng Tian, Yu Kong, Bineng Zhong, and Yun Fu. Residual dense network for image restoration. *IEEE Transactions on Pattern Analysis and Machine Intelligence*, 43(7):2480–2495, 2021. doi:<https://doi.org/10.1109/TPAMI.2020.2968521>.
- [35] Bo Fu, Xiaoyang Zhao, Yi Li, Xianghai Wang, and Yonggong Ren. A convolutional neural networks denoising approach for salt and pepper noise. *Multimedia Tools and Applications*, 78(21):30707–30721, Nov 2019. ISSN 1573-7721. doi:<https://doi.org/10.1007/s11042-018-6521-4>.
- [36] Krystian Radlak, Lukasz Malinski, and Bogdan Smolka. Deep learning based switching filter for impulsive noise removal in color images. *Sensors*, 20(10), 2020. ISSN 1424-8220. doi:<https://doi.org/10.3390/s20102782>.
- [37] Harold C. Burger, Christian J. Schuler, and Stefan Harmeling. Image denoising: Can plain neural networks compete with bm3d? In *2012 IEEE Conference on Computer Vision and Pattern Recognition*, pages 2392–2399, 2012. doi:<https://doi.org/10.1109/CVPR.2012.6247952>.
- [38] Jaakko Lehtinen, Jacob Munkberg, Jon Hasselgren, Samuli Laine, Tero Karras, Miika Aittala, and Timo Aila. Noise2noise: Learning image restoration without clean data. *arXiv preprint arXiv:1803.04189*, 2018. doi:<https://doi.org/10.48550/arXiv.1803.04189>.
- [39] Wenhua Zhang, Lianghai Jin, Enmin Song, and Xiangyang Xu. Removal of impulse noise in color images based on convolutional neural network. *Applied Soft Computing*, 82:105558, 2019. ISSN 1568-4946. doi:<https://doi.org/10.1016/j.asoc.2019.105558>.
- [40] Uğur Erkan, Dang Ngoc Hoang Thanh, Le Minh Hieu, and Serdar Enginoğlu. An iterative mean filter for image denoising. *IEEE Access*, 7:167847–167859, 2019. doi:<https://doi.org/10.1109/ACCESS.2019.2953924>.
- [41] Fengyu Chen, Minghui Huang, Zhuxi Ma, Yibo Li, and Qianbin Huang. An iterative weighted-mean filter for removal of high-density salt-and-pepper noise. *Symmetry*, 12(12), 2020. ISSN 2073-8994. doi:<https://doi.org/10.3390/sym12121990>.
- [42] Yunjin Chen and Thomas Pock. Trainable nonlinear reaction diffusion: A flexible framework for fast and effective image restoration. *IEEE Transactions on Pattern Analysis and Machine Intelligence*, 39(6):1256–1272, 2017. doi:<https://doi.org/10.1109/TPAMI.2016.2596743>.
- [43] D. Martin, C. Fowlkes, D. Tal, and J. Malik. A database of human segmented natural images and its application to evaluating segmentation algorithms and measuring ecological statistics. In *Proc. 8th Int’l Conf. Computer Vision*, volume 2, pages 416–423, July 2001.
- [44] Diederik P Kingma and Jimmy Ba. Adam: A method for stochastic optimization. In *International Conference on Learning Representations*, page 1–41, 2015.
- [45] Zhou Wang, A. C. Bovik, H. R. Sheikh, and E. P. Simoncelli. Image quality assessment: from error visibility to structural similarity. *IEEE Transactions on Image Processing*, 13(4):600–612, 2004. doi:<https://doi.org/10.1109/TIP.2003.819861>.

- [46] A. Horé and D. Ziou. Image quality metrics: PSNR vs. SSIM. In *20th International Conference on Pattern Recognition*, pages 2366–2369, 2010. doi:<https://doi.org/10.1109/ICPR.2010.579>.